Atmos. Chem. Phys., 10, 453–462, 2010
www.atmos-chem-phys.net/10/453/2010/


Atmospheric Chemistry and Physics

# Increasing synoptic scale variability in atmospheric $CO_2$ at Hateruma Island associated with increasing East-Asian emissions

**Y. Tohjima**[1], **H. Mukai**[2], **S. Hashimoto**[2], **and P. K. Patra**[3]

[1]Atmospheric Environment Division, National Institute for Environmental Studies, Tsukuba, Japan
[2]Center for Global Environmental Research, National Institute for Environmental Studies, Tsukuba, Japan
[3]Research Institute for Global Change, JAMSTEC, Yokohama, Japan

Received: 9 July 2009 – Published in Atmos. Chem. Phys. Discuss.: 24 July 2009
Revised: 11 December 2009 – Accepted: 16 December 2009 – Published: 19 January 2010

**Abstract.** In-situ observations of atmospheric $CO_2$ and $CH_4$ at Hateruma Island (24.05° N, 123.80° E, 47 m a.s.l), Japan shows large synoptic scale variations during a 6-month period from November to April, when the sampled air is predominantly of continental origin due to the Asian winter monsoon. Synoptic scale variations are extracted from the daily averaged values for the years between 1996 and 2007, along with the annual standard deviations ($\sigma_{CO_2}$ and $\sigma_{CH_4}$ for $CO_2$ and $CH_4$, respectively) for the relevant 6-month period. During this 6-month period the absolute mixing ratios of $CO_2$ and $CH_4$ at Hateruma are also elevated compared to those at two sites in the central North Pacific Ocean. The temporal change in $\sigma_{CO_2}$ shows a systematic increase over the 12-year period, with elevated excursions in 1998 and 2003; there is no clear increase in $\sigma_{CH_4}$. We also find that the $\sigma_{CO_2}/\sigma_{CH_4}$ ratio increases gradually from 1996 to 2002 and rapidly after 2002 without any extreme deviations that characterised $\sigma_{CO_2}$. The $\sigma_{CO_2}/\sigma_{CH_4}$ ratio correlates closely with the recent rapid increase in fossil carbon emissions from China, as indicated in the Carbon Dioxide Information Analysis Center (CDIAC) database. This methodology can be applied to multiple chemical tracers of sufficient lifetime, for tracking overall changes in regional emissions.

*Correspondence to:* Y. Tohjima
(tohjima@nies.go.jp)

## 1 Introduction

The increase in carbon dioxide ($CO_2$) emissions from fossil fuel consumption, cement manufacturing and decomposition of biomass and soil organic matter associated with land-use changes has contributed to the observed rise in atmospheric $CO_2$ since the industrial revolution (Marland et al., 2007; Houghton, 2003). Although, on average, more than half of the anthropogenic $CO_2$ has been taken up by the land biosphere and the ocean (Tans et al., 1990), the recent growth rate of atmospheric $CO_2$ shows a gradual increasing trend mainly due to the continuous increase in fossil fuel consumption (e.g. Keeling et al., 1995; Patra et al., 2005). Despite international discussions to reduce greenhouse gas emissions, global $CO_2$ emissions from fossil fuel consumption and cement manufacturing derived from the CDIAC database (Marland et al., 2007) show an unprecedented accelerated growth during the period 2002–2006. This rapid emission growth has been attributed to the accelerating emissions from the developing countries, especially China (Raupach et al., 2007; Gregg et al., 2008).

Increasing fossil fuel $CO_2$ emissions in East Asia elevate not only the overall global atmospheric burden but also enhance the local atmospheric mixing ratios relative to the surrounding regions. Thus, a greater emission intensity will produce a larger mixing ratio gradient in the downwind region, resulting in a greater synoptic scale variation (SSV) in the $CO_2$ mixing ratios when synoptic scale winds change direction. For example, the Chinese $CO_2$ emission data from the CDIAC database indicate a rapid increase from 0.9 Pg-C in 2000 to 1.7 Pg-C in 2006, which could affect the SSVs in East Asia. Since the amplitude of SSVs will likely change as a function of the source-receptor distance and the source

Published by Copernicus Publications on behalf of the European Geosciences Union.

strength, a SSV ratio of two chemical tracers (such as $CO_2$ and $CH_4$ employed in this study) with a similar emission pattern and long instantaneous lifetime (∼month-year) would conserve the ratio of the source strengths robustly.

The National Institute for Environmental Studies (NIES) has been carrying out in-situ measurements of atmospheric greenhouse gases, including $CO_2$, since October 1993 and methane ($CH_4$) since January 1996 at Hateruma Island (HAT; 24.05° N, 123.80° E, 47 m above sea level (a.s.l)), which is located on the East-Asian continental margin. The observations at HAT often show pollution events influenced by continental emissions during the period from the late fall to early spring each year (Tohjima et al., 2000, 2002; Yokouchi et al., 2006). Recently, analyses of the SSVs have been found to be useful for validating regional fluxes with the help of a chemistry-transport model (Patra et al., 2009). In this paper, we examine the temporal changes in atmospheric $CO_2$ SSVs observed at HAT in wintertime (November–April) during 1996–2007 and investigate their relationship to the continental fossil $CO_2$ emissions. The $CO_2$ SSVs are usually associated with similar SSVs in $CH_4$ observed at HAT. Therefore, the ratio of $CO_2$ and $CH_4$ SSVs is used to construct a conservative tracer for tracking emission changes over the source regions.

## 2 Data and methods

We use daily averages of the atmospheric $CO_2$ and $CH_4$ mixing ratios observed at HAT. The $CO_2$ mixing ratios were continuously measured by a nondispersive infrared analyzer (NDIR) (Mukai et al., 2001) and the $CH_4$ mixing ratios were semi-continuously measured by a gas chromatography equipped with a flame ionization detector (FID) (Tohjima et al., 2002). Both $CO_2$ and $CH_4$ values are reported on the NIES gravimetric standard scales (NIES-95 $CO_2$ and $CH_4$ scale) (Machida et al., 2009; Tohjima et al., 2002). The 4th WMO Round-Robin reference gas intercomparison program revealed that the differences in $CO_2$ and $CH_4$ between the WMO scale and the NIES 95 scale (NIES-WMO) are −0.10 to −0.14 ppm in a range between 355 and 385 ppm and +4 to +5 ppb in a range between 1750 and 1838 ppb, respectively (Zhou et al., 2009). The $CO_2$ and $CH_4$ data at HAT are submitted to the World Data Center for Greenhouse Gases (WDCGG; http://gaw.kishou.go.jp/wdcgg/) of the World Meteorological Organization (WMO) and GLOBALVIEW-$CO_2$/$CH_4$ database (www.esrl.noaa.gov/gmd/ccgg/globalview/). The $CO_2$ and $CH_4$ time series from this site have been used successfully in studies involving data from multiple organizations (see Law et al., 2008; Patra et al., 2008, 2009).

To characterise the air mass transport to HAT, we calculate kinematic 3-day backward trajectories with an arrival time of 06:00 UTC (15:00 JST) and starting altitude of 500 m a.s.l by using the METEX (METeorological data EXplorer, http://db.cger.nies.go.jp/metex/) programme developed by Zeng et al. (2003). In the trajectory calculations, the National Center for Environmental Prediction (NCEP) reanalysis data with time resolution of 6 h, latitude/longitude grid of 2.5 degree and 17 pressure levels are used (Kistler et al., 2001).

The observed $CO_2$ and $CH_4$ variations include not only SSVs but also long-term trends and regular and irregular seasonal variations. To remove the seasonal variations and the long-term trend from the observed $CO_2$ and $CH_4$ data, we first obtain smooth-curve fits to the data following the methods of Thoning et al. (1989) with a cut-off frequency of 4.6 cycles $yr^{-1}$, roughly corresponding to a 40-day running average. Then we subtract the smooth-curve fits from the original time series to extract the SSV components, which are denoted by the $\Delta$ notation as $\Delta CO_2$ and $\Delta CH_4$ (similar to that used in Patra et al., 2008). To express the molar mixing ratios, we use the units of μmol $mol^{-1}$ (ppm) for $CO_2$ and nmol $mol^{-1}$ (ppb) for $CH_4$. Figure 1 depicts the time series of $\Delta CO_2$ and $\Delta CH_4$ in 2000 as a typical example. It should be noted that these time series show noticeably similar variations during the periods from January to April and from November to December. Annual standard deviations of $\Delta CO_2$ and $\Delta CH_4$ (defined as $\sigma_{CO_2}$ and $\sigma_{CH_4}$) are calculated using the data from January to April and from November to December. The data for the period May to October are not used in this study. We also investigate the ratio of $\sigma_{CO_2}$ to $\sigma_{CH_4}$. Note that the daily data are applied to these analyses only when both $CO_2$ and $CH_4$ data exist.

We extend the analysis of the observed SSVs by simulating the daily averages of $CO_2$ and $CH_4$ at HAT with an atmospheric general circulation model (AGCM) based chemistry-transport model (ACTM). ACTM runs at a horizontal resolution of T42 spectral truncation (∼ 2.8° × 2.8°) and 67 sigma-pressure vertical layers. The transport model is driven by the Centre for Climate System Research/National Institute for Environmental Studies/Frontier Research Centre for Global Change AGCM, nudged with horizontal winds and temperature from the National Centre for Environmental Prediction reanalysis II (NCEP2; Kanamitsu et al., 2002). The modelling period is from January 1990 to December 2006, and the first six years are a spin-up period, during which long-term transport mechanisms, such as the inter-hemispheric gradient and stratosphere-troposphere exchange, are equilibrated in the model. The capability of the ACTM to simulate $CO_2$ and $CH_4$ has been investigated elsewhere (Patra et al., 2008, 2009). We use the $CH_4$ emission scenario (E2 scenario) developed in Patra et al. (2009) that optimally fits the interhemispheric gradient and seasonal cycles at most sites around the globe to within 10 ppb on average. For the $CO_2$ simulation, annually balanced terrestrial ecosystem flux (Randerson et al., 1997), oceanic exchange (Takahashi et al., 2009) and fossil fuel emissions are used simultaneously. While the monthly-mean terrestrial and oceanic fluxes are repeated every year, the annual-mean

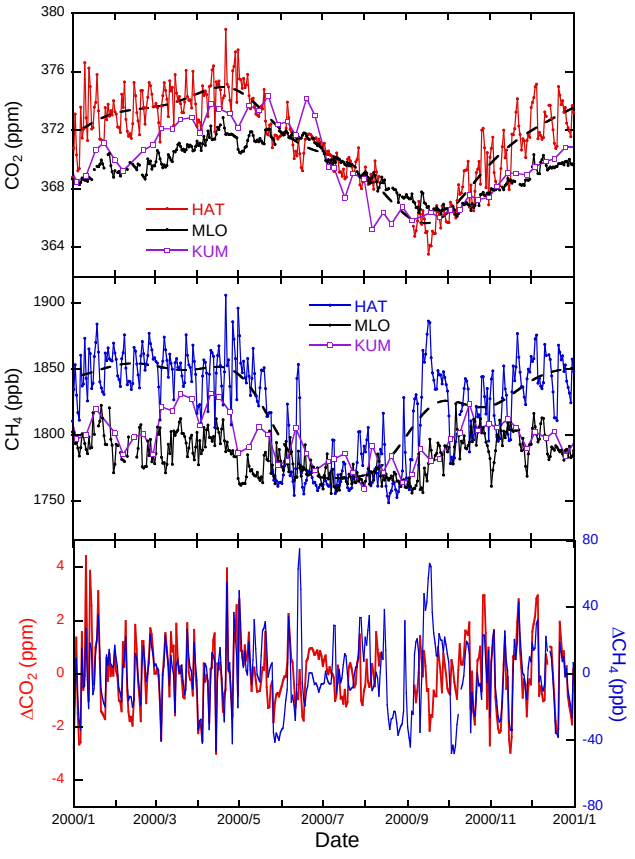


**Fig. 1.** Time series of (top) the daily averages of $CO_2$, (middle) daily averages of $CH_4$, and (bottom) the synoptic scale variations (SSVs) in $CO_2$, ($\Delta CO_2$, red, left axis) and $CH_4$, ($\Delta CH_4$, blue, right axis) observed at HAT in 2000. The daily averages of $CO_2$ and $CH_4$ at MLO (black line) and KUM (purple line with open squares), measured by NOAA/ESRL GMD, are also plotted for the comparison. The broken lines represent the smooth-curve fits to the observed $CO_2$ and $CH_4$ data at HAT. $\Delta CO_2$ and $\Delta CH_4$ are defined as differences between the daily averages and the smooth curve fits to the observed data (see text).

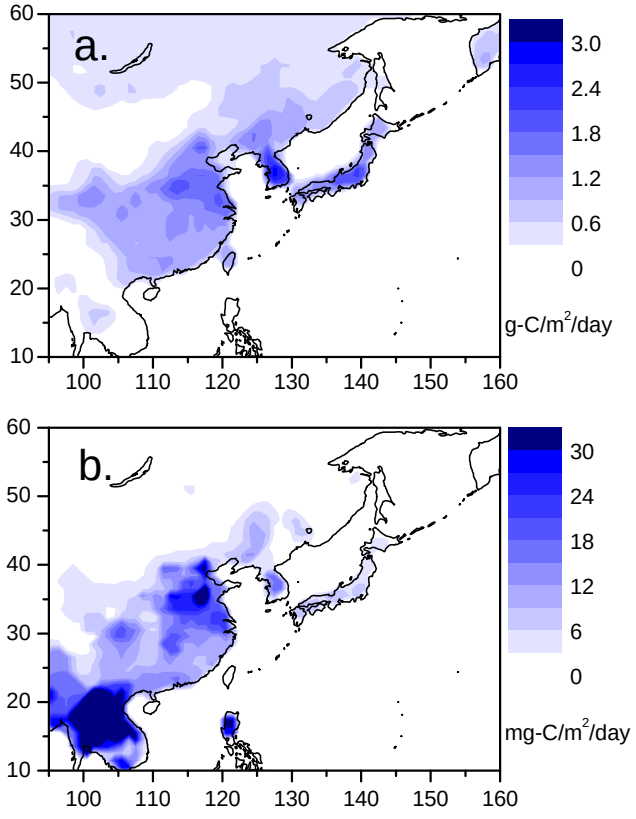


**Fig. 2.** The spatial distributions of **(a)** $CO_2$ and **(b)** $CH_4$ fluxes used in the model simulation of this study. Both fluxes are averaged during six months (January–April and November–December) in 2000.

fossil flux is increased/decreased year-to-year. The fossil fuel fluxes are developed as follows: first spatial distribution of anthropogenic $CO_2$ emission are constructed for the period of 1990–2000 by interpolating the emissions maps for the years 1990, 1995 and 2000 based on EDGAR3.2 (Olivier and Berdowski, 2001) and EDGAR32FT2000 (Olivier et al., 2005). For the years after 2000, the EDGAR32FT2000 map is used. Then we used the national total emission inventories from CDIAC database corresponding to each year for the period of our simulation to scale the emission maps. The spatial distributions of total $CO_2$ and $CH_4$ fluxes averaged during six months (January–April and November–December) in 2000 are shown in Fig. 2.

## 3 Results

The daily averages of $CO_2$ and $CH_4$, using the continuous observations at HAT in 2000, are shown in Fig. 1 together with the $CO_2$ and $CH_4$ data at Mauna Loa (MLO; 19.5° N, 155.6° W, 3397 m a.s.l) measured by the Global Monitoring Division of the National Oceanic and Atmospheric Administration's Earth System Research Laboratory (NOAA/ESRL GMD) (Thoning et al., 1989; Dlugokencky et al., 1995). The levels of $CO_2$ and $CH_4$ mixing ratios at HAT are greater than those at MLO during the period of our analysis (November–April). This gradient in mixing ratio between HAT and MLO is caused by the high continental emissions and the prevailing northwesterly winds across East Asia, compared to the tropics of the North Pacific Ocean. During the summer months, when both the continent and the ocean act as net sinks of $CO_2$, and when $CH_4$ chemical loss due to its reaction with OH is strongest, the gradient between HAT and MLO tends to disappear. Because MLO is a high altitude site, some differences between MLO and HAT observations may arise from mixing ratio gradients with altitude as noted in earlier studies (Dlugokencky et al., 1995; Thoning et al., 1989). Thus, we also show discrete observations using flask

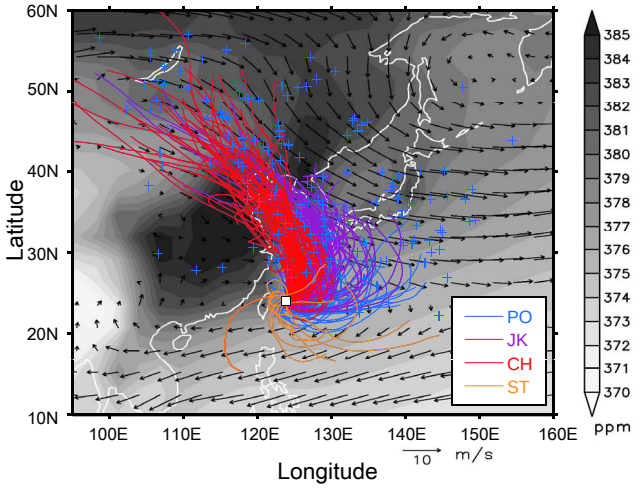


**Fig. 3.** Three-day backward trajectories for air masses arriving at HAT during the 6 months (January–April and November–December) in 2000. The arrival time of the trajectories is 06:00 UTC (15:00 JST). The air mass origins are categorized into 4 regions: China (CH, red), Japan and Korea (JK, purple), subtropics (ST, orange), and Pacific Ocean (PO, blue). Blue cross symbols represent the 4, 5, 6, and 7-day upwind positions of the backward trajectories for PO. The distribution of the simulated mean $CO_2$ mixing ratio at the Earth's surface and mean wind vectors (in $m\,s^{-1}$, see legend) at 850 mb height for the 3 months (December–February) are also depicted.

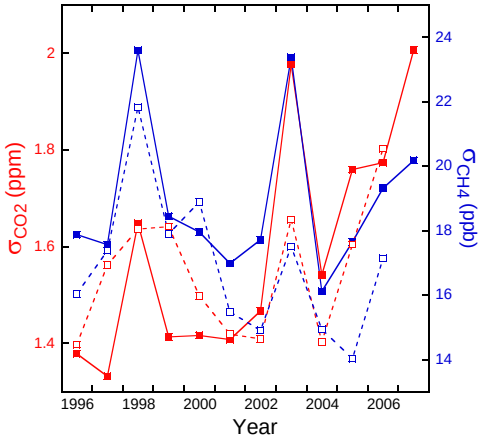


**Fig. 4.** Temporal changes in the standard deviations of $\Delta CO_2$ ($\sigma_{CO_2}$, red) and $\Delta CH_4$ ($\sigma_{CH_4}$, blue) based on the data from January to April and from November to December. Closed symbols with solid lines correspond to the observation and open symbols with broken lines correspond to the model simulation.

samples from a surface site, Cape Kumukahi (KUM; 19.5° N, 154.8° W, 3 m a.s.l) in Fig. 1 (Conway et al., 1994; Dlugokencky et al., 1994). Though synoptic variations cannot be seen in the KUM time series, due to coarse time resolution of the data (weekly intervals), we find the average values (as shown by the broken line) at HAT are always higher than mixing ratios observed at KUM during November–April. However, detailed discussion of the differences between the time series at these two sites is beyond the scope of this study.

The backward trajectories of the air masses arriving at HAT in 2000 during the 6-month period (January–April and November–December) are depicted in Fig. 3. During this period, observations at HAT are dominantly influenced by the air masses transported from the East-Asian continental regions. On the other hand, the maritime air masses over the Pacific Ocean are dominantly transported to the site during the period from May to October. (trajectories not shown). Such clear transport patterns are caused by the East-Asian winter monsoon and are climatologically characteristic of this region (Newell and Evans, 2000; Tohjima et al., 2000, 2002). Because the November–April period is biologically dormant, limiting our analysis to this period has an advantage of reduced, if not negligible, influence from interannual variations in the land biosphere-atmosphere $CO_2$ exchange. A more detailed investigation of the backward trajectories shows that the observations at HAT are affected by the emissions from the provinces around Beijing (21±4%), along the east coast of China around Shanghai (17±4%), Korea (12±3%), and the southern part of Japan (12±4%), where numbers in the parentheses represent the average and standard deviation of the number of trajectories per year originating in these source regions. The positive $\Delta CO_2$ value is produced mostly when the air mass is directly transported from the source regions, while the negative $\Delta CO_2$ value is associated with the air mass that travels longer over the ocean, circling clockwise around the site. Similar conditions characterise the atmospheric $CH_4$ SSV peaks throughout the year since $CH_4$ has a similar emission pattern. Although HAT Island is located in the western North Pacific region with a lot of ship traffic that emits $CO_2$ (Eyring et al., 2010) and is also likely to produce peaks in $CO_2$ time series, we examined observations at hourly intervals but did not find evidence for short-lived ship plumes at HAT. The $CO_2$ deviations occurred on much longer time scales and are indicative of the emissions from continental sources of greater emission strength.

The temporal changes in $\sigma_{CO_2}$ and $\sigma_{CH_4}$ are shown in Fig. 4. There are large interannual variations in both $\sigma$ time-series; especially the simultaneous abrupt enhancements in 1998 and 2003 are noteworthy. However, if we exclude the anomalously high $\sigma_{CO_2}$ values in 1998 and 2003, the data show a gradual increase during 1996–2002 and a sharp rise during 2002–2007, resembling the growth rate of estimated annual-total fossil $CO_2$ emission from China (see Fig. 5). On the other hand, the temporal changes in $\sigma_{CH_4}$ do not show a clear increase or decrease, after the anomalous $\sigma_{CH_4}$ values in 1998 and 2003 are removed.

Figure 5 shows a time variation in the $\sigma_{CO_2}/\sigma_{CH_4}$ ratio as a robust estimation of relative change in emissions (red squares). For instance, continuous or episodic transport from

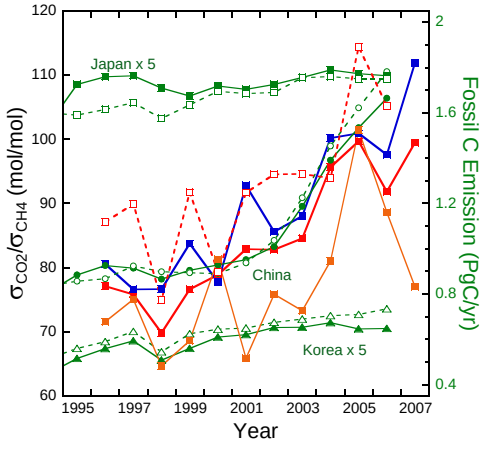


**Fig. 5.** Temporal changes in the $\sigma_{CO_2}/\sigma_{CH_4}$ ratio for all observation data (closed red squares), limited observation data corresponding to the air masses originating in CH and PO (closed blue squares) and originating in JK and ST (closed orange squares), and all simulation data (open red squares). Green symbols represent the national carbon emissions from fossil fuel consumption and cement manufacturing for China (circles), Japan (squares), and Korea (triangles). The carbon emission data obtained from CDIAC are depicted as solid symbols and those based on EIA as open symbols. Carbon emissions from cement production in the CDIAC dataset are added to those from EIA dataset. The values of the carbon emission from Korea and Japan are multiplied by 5.

the source region to the measurement site will decrease or increase the SSV peak magnitudes, respectively. By normalizing $\sigma_{CO_2}$ with respect to $\sigma_{CH_4}$ interannual transport variations would be eliminated. However, disproportional changes in the emission ratio of $CO_2$ and $CH_4$ would still show up, likely contributing to the differences in the SSV increase for $CH_4$ and $CO_2$ in 1998 and 2003, or the appearance of interannual variations in the $\sigma_{CO_2}/\sigma_{CH_4}$ ratio time series (given the fact that the emission distribution of the two species are not exactly the same). The interannual variability in the ratio is substantially reduced in comparison with $\sigma_{CO_2}$ and the ratio clearly shows a steady increase. For comparison, annual time series of national carbon emissions from fossil fuel combustion and cement production for China, Japan and Korea taken from the CDIAC database (1996–2006) and the US Department of Energy Energy Information Administration (EIA, www.eia.doe.gov) database (1996–2006) are also plotted in Fig. 5. Note that the carbon emissions from cement production in the CDIAC dataset are added to the EIA dataset and that the emissions from Japan and Korea, shown in Fig. 5, are multiplied by a factor of 5. The national emissions from CDIAC and EIA agree with each other to within ∼7% for China, ∼8% for Japan and ∼13% for Korea. There is a good agreement between the temporal changes in the $\sigma_{CO_2}/\sigma_{CH_4}$ ratio and fossil carbon emission from China: both temporal changes show a gradual increase during 1996–2002 and a rapid increase during 2002–2005, especially in 2004. While

**Table 1.** Summary of squared correlation coefficients ($r^2$) of $\sigma_{CO_2}/\sigma_{CH_4}$ and $\sigma_{CO_2}$ with the national carbon emissions.

| | $\sigma_{CO_2}/\sigma_{CH_4}$ | | | | $\sigma_{CO_2}$ | | | |
|---|---|---|---|---|---|---|---|---|
| Country | CDIAC 96-05 | CDIAC 96-06 | EIA 96-05 | EIA 96-06 | CDIAC 96-96 | CDIAC 96-96[a] | EIA 96-96 | EIA 96-06[a] |
| China | 0.91[b] | 0.81[b] | 0.88[b] | 0.78[b] | 0.41[c] | 0.92[b] | 0.44[c] | 0.92[b] |
| Japan | 0.37 | 0.40[c] | 0.76[b] | 0.79[b] | 0.12 | 0.21 | 0.31 | 0.66[d] |
| Korea | 0.67[d] | 0.68[d] | 0.77[b] | 0.78[b] | 0.13 | 0.39[c] | 0.21 | 0.76[b] |

[a] The correlation coefficients are calculated except for the $\sigma_{CO_2}$ values in 1998 and 2003. [b] Values statistically significant at $p < 0.001$. [c] Values statistically significant at $p < 0.05$. [d] Values with $p < 0.01$.

the EIA dataset for China still shows growing emissions in 2006, the observed $\sigma_{CO_2}/\sigma_{CH_4}$ ratio shows a considerable decrease in 2006.

The time series of $\sigma_{CO_2}$ and $\sigma_{CH_4}$ and the $\sigma_{CO_2}/\sigma_{CH_4}$ ratio based on the simulated $CO_2$ and $CH_4$ are also depicted in Fig. 4 and 5, respectively, as open symbols with broken lines. The temporal changes in $\sigma_{CO_2}$ and $\sigma_{CH_4}$ produced by the model simulation also show anomalies in 1998 and 2003, although the amplitude of both $CO_2$ and $CH_4$ variations are smaller in 2003 in comparison with the observation. The temporal changes in the $\sigma_{CO_2}/\sigma_{CH_4}$ ratio show a better correspondence between the model simulation and the observation than those for $\sigma_{CO_2}$ and $\sigma_{CH_4}$. This result suggests the effectiveness of the normalization of $\sigma_{CO_2}$ with respect to $\sigma_{CH_4}$ to reduce the transport effect. To clarify the impact of fossil fuel emissions on the change in the simulated $\sigma_{CO_2}/\sigma_{CH_4}$ ratio, we depict two time series of the simulated $\sigma_{CO_2}/\sigma_{CH_4}$ ratios based on the fossil fuel $CO_2$ component and the terrestrial ecosystem $CO_2$ component in Fig. 6. The fossil fuel component shows a clear increase while the temporal change in the terrestrial component is unclear. Since only the fossil $CO_2$ flux has year-to-year changes derived from the CDIAC database, this result indicates that in the temporal change in the simulated $\sigma_{CO_2}/\sigma_{CH_4}$ ratio mostly reflects the fossil flux change.

Squared Pearson correlation coefficients ($r^2$) of the observed $\sigma_{CO_2}/\sigma_{CH_4}$ ratio and the $\sigma_{CO_2}$ values with the reported fossil carbon emissions from China, Japan and Korea are summarized in Table 1. Most of the correlations are statistically significant ($p < 0.05$). For the $\sigma_{CO_2}/\sigma_{CH_4}$ ratio, emissions from China for 1996–2005 based on both the CDIAC and EIA data account for the highest portion of the temporal variation. However, when emissions for 2006 are included, correlation coefficients between the $\sigma_{CO_2}/\sigma_{CH_4}$ ratio and emissions from China are slightly reduced because of the sudden decrease in the $\sigma_{CO_2}/\sigma_{CH_4}$ ratio and the continued increase in emissions in 2006. On the other hand, although the temporal changes in the $\sigma_{CO_2}$ values also show the highest correlation with emissions from China, the correlation coefficients are much lower than those for the $\sigma_{CO_2}/\sigma_{CH_4}$ ratio. However, if the anomalous values of 1998 and 2003 are

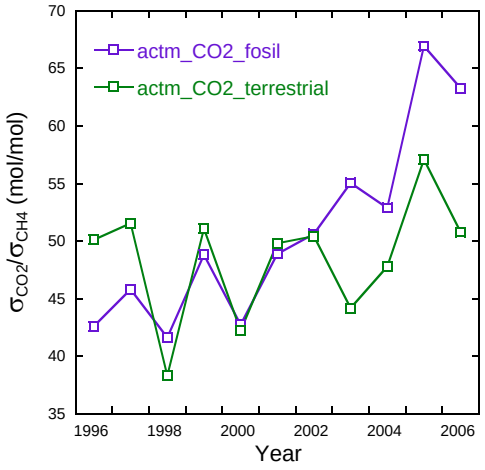


**Fig. 6.** Temporal changes in the simulated $\sigma_{CO_2}/\sigma_{CH_4}$ ratios at HAT based on the fossil fuel $CO_2$ component (purple squares) and the terrestrial ecosystem $CO_2$ component (green circles).

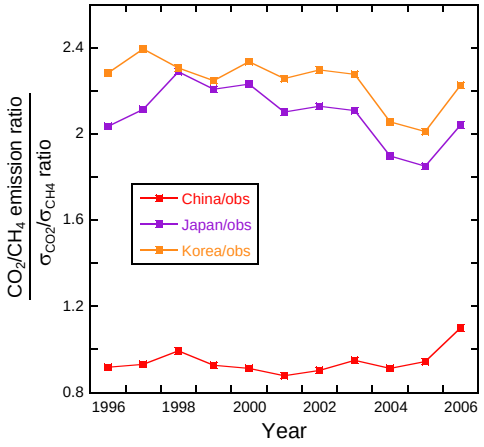


**Fig. 7.** Interannual variation in the national $CO_2/CH_4$ emission ratio for China (red), Japan (purple) and Korea (orange) normalized by the $\sigma_{CO_2}/\sigma_{CH_4}$ ratio at HAT. The national $CO_2/CH_4$ emission ratios are calculated from the November-to-April monthly fluxes used in the model simulation.

removed, the correlation between the $\sigma_{CO_2}$ values and the emissions from China increases to 0.92 for both the CDIAC and EIA data even if the $\sigma_{CO_2}$ value in 2006 is included. Furthermore, the national emission ratio of $CO_2$ to $CH_4$ for China, based on the November–April monthly fluxes used in the model simulation, is almost identical to the $\sigma_{CO_2}/\sigma_{CH_4}$ ratio at HAT, while those for Japan and Korea are more than double. Moreover, the relative change in the national emission ratio ($CO_2/CH_4$) for China against the $\sigma_{CO_2}/\sigma_{CH_4}$ ratio is almost constant ($\sim$1) during 1996–2005, while those for Japan and Korea show a gradual decrease (Fig. 7). These results strongly suggest that the SSVs at HAT are affected predominantly by the emissions from China.

## 4 Discussion

The years of 1997/1998 and 2002/2003 correspond to strong and moderate El Niño periods, respectively. El Niño events alter wind and radiation (outgoing long-wave readiation (OLR), for example) patterns (Trenberth, 1997), causing anomalous transport and anomalous enhancement of $CO_2$ and $CH_4$ mixing ratios in the source region that could explain the enhanced variability in $CO_2$ and $CH_4$ at HAT observed in 1998 and 2003. For example, the differences in the $CO_2$ and $CH_4$ mixing ratios at the surface, wind vectors and outgoing longwave radiation (OLR) between the periods of December 2001 to February 2002 and December 2002 to February 2003, respectively, are depicted in Fig. 8 as simulated by ACTM. Indeed, a relatively good qualitative agreement between the ACTM simulated and observed variations in $\sigma_{CH_4}$ at HAT (Fig. 4) is indicative of the significant role the interannual transport variation plays in causing the observed interannual synoptic-scale variation, since nearly constant $CH_4$ emissions are used in the model, as well as the neglect of the interannual variation in OH (Patra et al., 2009). The $\sigma_{CO_2}/\sigma_{CH_4}$ ratio reduces this transport effect, as noted earlier. We also contend that, within the confines of our study, any change in the $\sigma_{CO_2}/\sigma_{CH_4}$ ratio is mostly reflective of a change in fossil fuel $CO_2$ emissions. Although interannual climate variations in such parameters as land temperature and precipitation, or in biomass burning can lead to disproportionate release/uptake of $CO_2$ and $CH_4$ due to the differences in the emission factors associated with different land surfaces (e.g., wetland area, agricultural land), ecosystem types (e.g., grassland, savannah, tree) and processes involved (Andreae and Merlet, 2001), we will argue below that these have only secondary effects on our results.

Past El Niño events have certainly influenced the global sources of $CH_4$ and $CO_2$ in various ways. For example, unusually large boreal forest fires in eastern Russia from May to October in 1998 and 2002/2003 (Kasischke et al., 2005; Patra et al., 2005) would have contributed to the enhancement of $\sigma_{CO_2}$ and $\sigma_{CH_4}$, but since these events occurred outside of the 6-month period under study, the impact of the biomass burning on our result regarding the $\sigma_{CO_2}/\sigma_{CH_4}$ ratio is minimal. Similarly, the $CH_4$ emissions from seasonal sources including wetlands and rice fields in East Asia during the analysis period (November–April) are much smaller than the emissions from the year-round non-seasonal sources including livestock, energy use (coal and natural gas) and landfills. For example, $CH_4$ emission from Chinese rice fields occurs from April to November, with more than 70% of emissions occurring between June and August and maximum emissions observed in August (Yan et al., 2003). In addition, the growth rate of the global atmospheric $CH_4$ concentration decreased after 1980, confined between $\pm$5 ppb/yr during 1996–2005 (with the exception of 1998) (Simpson et

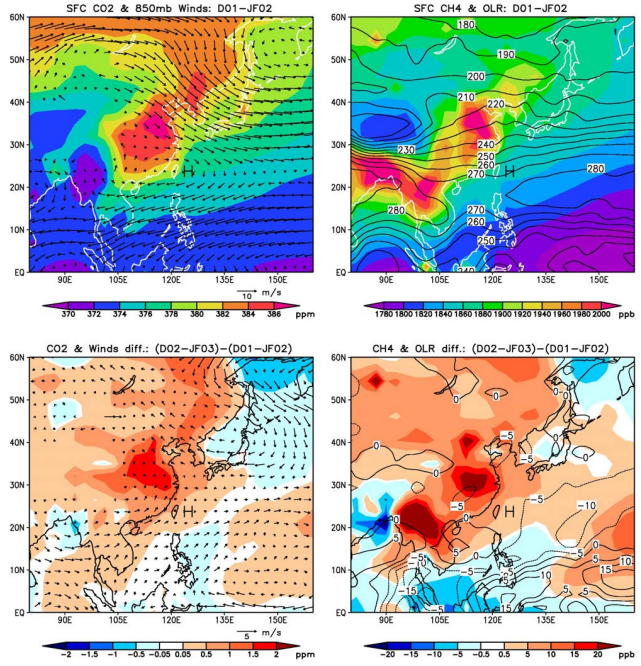


**Fig. 8.** Examples of 3-monthly (December–February) mean ACTM simulations over the East-Asian region. The distributions of $CO_2$ at surface and wind vectors (in m s$^{-1}$, see legend) (top left), $CH_4$ at surface and outgoing longwave radiation (OLR in W m$^{-2}$; contoured) (top right), interannual differences in $CO_2$ at surface and wind vectors (bottom left) and interannual differences in $CH_4$ at surface and OLR (bottom right). The results shown in the top and bottom diagrams correspond to 3-monthly means from December 2001 to February 2002 and the differences between the periods December 2001 to February 2002 and December 2002 to February 2003, respectively.

al., 2006; Dlugokencky et al. 2009), unlike the rapidly increasing $CO_2$ from fossil fuel sources. A forward model simulation shows that a nearly constant global $CH_4$ emission during 1995–2006 is able to reproduce the observed atmospheric $CH_4$ change with a fixed OH distribution (Patra et al., 2009), supporting the idea of a recent stable $CH_4$ source strength. Anthropogenic $CH_4$ emission estimates from REAS 1.11 (Regional Emission inventory in ASia) (Ohara et al., 2007) also show that the variability in the estimated yearly anthropogenic $CH_4$ emission from China is less than ± 3%. Furthermore, there is little photosynthetic uptake to the $CO_2$ emissions from East Asia during the 6-month study period; heterotrophic respiration is also relatively small during the colder 6-month period compared to the rest of the year (Ito, 2008). It is our contention that the above discussions lend sufficient support to our assumption that the observed $\sigma_{CO_2}/\sigma_{CH_4}$ ratio for the seasonal period of November to April at HAT is predominantly reflective of the changes in fossil $CO_2$ emissions in East Asia.

To investigate the influence of the regional $CO_2$ emission variation to the SSVs at HAT, we categorize the origins of

**Table 2.** Percent frequency of occurrence of the 4 air mass origins for the 3 percentile rages of $\Delta CO_2$ and statistics of $\Delta CO_2$ for the individual air mass origins[a]

| Air mass origin | Frequency of occurrence (in %) | | | $\Delta CO_2$[b] | | |
|---|---|---|---|---|---|---|
| | 0∼33[c] | 34∼66[c] | 67∼100[c] | Average | 1 SD | N |
| CH | 17.7 | 38.4 | 57.9 | 0.71 | 1.58 | 806 |
| JK | 18.9 | 31.0 | 21.3 | −0.03 | 1.13 | 507 |
| ST | 18.1 | 5.3 | 3.7 | −1.13 | 1.77 | 195 |
| PO | 45.2 | 25.4 | 17.1 | −0.60 | 1.44 | 628 |

[a] Values are based on the data from six months (January–April and November–December) during 1996–2007. [b] Values for average and standard deviation (1 SD) are given in ppm. [c] Percentile range of $\Delta CO_2$.

the air masses arriving at HAT into 4 regions (China (CH), Japan and Korea (JK), the subtropics (ST), and the Pacific Ocean (PO)) by using the 3-day backward trajectories. We designate the trajectory as CH, JK and ST when the 3-day backward trajectory first crosses the corresponding regional boundaries. The remaining trajectories are designated as PO. In this study, the regional boundaries for CH and JK are the borders of the corresponding countries with a resolution of 1×1° degree, and for ST the border of Taiwan and latitude of 20° N. The results of the categorization of the backward trajectories for 2000 are also illustrated by different colours in Fig. 3. The percentages of the trajectories occurring in these categorized origins are 38±5%, 24±5%, 9±4%, and 29±4% for CH, JK, ST and PO, respectively. We divide $\Delta CO_2$ data into 3 groups according to the percentile ranges (0∼33, 34∼66 and 67∼100) and calculate the frequencies of occurrence (in %) for the 4 air mass origins in each $\Delta CO_2$ group. The results are summarized in Table 2. The highest frequency (58%) for CH is found in the upper third $\Delta CO_2$ group while those for ST and PO are found in the lower third $\Delta CO_2$ group. The average $\Delta CO_2$ values for the individual air mass groups (Table 2) generally follow the regional emission strength (CH>JK>PO>ST). The negative $\Delta CO_2$ indicates that trajectories, originating in PO and ST, bring air mass with lower $CO_2$ concentrations compared to the average background concentration at HAT.

Temporal variation in $\sigma_{CO_2}$ associated with each of the geographical categories is plotted in Fig. 9, together with that derived from all $\Delta CO_2$. The change observed in $\sigma_{CO_2}$ for CH shows an increase that is similar to the overall change. Although PO is considered to be background region for $CO_2$ without any strong sources, the $\sigma_{CO_2}$ time series for PO also shows an increase similar to that for CH. Since the fossil $CO_2$ emissions from China are substantially large, the increase in PO $\sigma_{CO_2}$ suggests that the air masses transported from PO region are, to some extent, influenced by the emissions from China (Fig. 8). Actually, most of the air masses designated as PO origin finally reach the East-Asian continental region when the backward duration for the trajectory calculation is extended to about a week, as shown in Fig. 3, where the 4–6

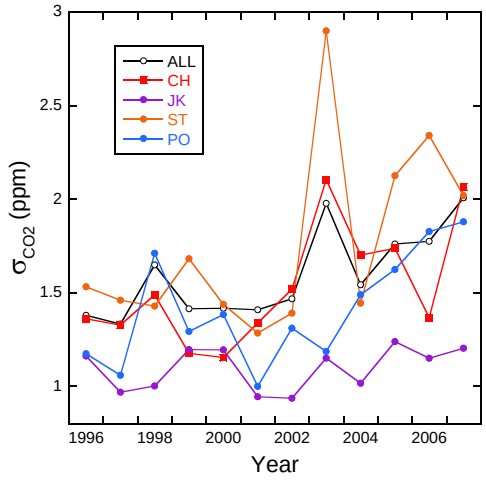


**Fig. 9.** Temporal changes in the $\sigma_{CO_2}$ values for the datasets categorized according to the four air mass origins. The $\sigma_{CO_2}$ values for all data are also depicted as open circle.

and 7-day upwind positions of the backward trajectories for PO are plotted as blue cross symbols. Although the $\sigma_{CO_2}$ for ST appears to show similar increase, the variability is apparently large. The $CO_2$ mixing ratios for the subtropical region are generally lower than those for the mid latitudes for the seasons of this analysis as shown in Table 2. Therefore, the latitudinal $CO_2$ gradient contributes to the large variability in $\sigma_{CO_2}$ for ST. The pollution episodes, attributed to emissions from Taiwan, may also contribute to the large variability. On the other hand, the $\sigma_{CO_2}$ time series for JK shows nearly no increase/decrease during the entire 12-year period. This result seems to be consistent with the changes in the recent fossil $CO_2$ emission from Japan and Korea. The air masses of JK origin should be influenced more strongly by the emissions from Japan and Korea than from China.

The range of transport pathways to HAT, indicated by the backward trajectories, covers some of the major $CO_2$ emission centres in China, including the provinces around Beijing and along the east coast of China (Gregg et al., 2008). This may be the reason why the $\sigma_{CO_2}/\sigma_{CH_4}$ ratio at HAT appears to closely track the pattern of the $CO_2$ emission increase from China during the period from 1996 to 2005, as indicated in the recently revised version of the CDIAC data used in this study (Marland et al., 2007). In the previous version of the CDIAC data, emissions from China decreased by about 20% during 1996–2000, which was mainly based on the official Chinese statistics reporting substantial reductions in fuel consumption, coal consumption in particular, during the aforementioned period. Several researchers questioned the official statistics based on the investigations of various energy statistics and the satellite observations of $NO_2$ over China (Akimoto et al., 2006; Zhang et al., 2007). The gradual increase during 1996–2002 and the rapid increase thereafter in the $\sigma_{CO_2}/\sigma_{CH_4}$ ratio at HAT support the recently revised Chinese emissions reflected in the CDIAC data.

The values of the $\sigma_{CO_2}/\sigma_{CH_4}$ ratio at HAT in 2006 and 2007 are considerably lower than and similar to the ratio observed in 2005, respectively. These temporal changes seem to suggest that the increasing rate of fossil $CO_2$ from China slowed down. However, plotting the values of the $\sigma_{CO_2}/\sigma_{CH_4}$ ratio, using those associated with air masses originating from CH and PO, as shown in Fig. 5 (blue squares), we find that the $\sigma_{CO_2}/\sigma_{CH_4}$ ratio for 2007 is higher than that for 2005, although the dip in 2006 is still present. On the other hand, the values of the $\sigma_{CO_2}/\sigma_{CH_4}$ ratio for JK and ST, also plotted in Fig. 5 (orange squares), are usually lower than those for all air mass origins and the discrepancy is the largest in 2007. This result is consistent with the largest $\sigma_{CO_2}/\sigma_{CH_4}$ ratio in 2007 for the air masses of CH and PO origins. We believe that the $\sigma_{CO_2}/\sigma_{CH_4}$ values for the air masses of CH and PO better reflect the emissions from China than those for all air mass origins. In addition, since $\sigma_{CO_2}$ shows the highest value in 2007 (Fig. 4), it is likely that the greater rate of the fossil $CO_2$ emissions from China continued through 2007, although the sharp dip in the $\sigma_{CO_2}/\sigma_{CH_4}$ ratio in 2006 is still difficult to explain at this time.

*Acknowledgements.* We gratefully acknowledge Nobukazu Oda and other staff members of the Global Environment Forum and the staff of Center for Global Environmental Research for their continued support in maintaining the in-situ measurements of $CO_2$ and $CH_4$ at HAT. We also thank Toshinobu Machida, Tomonori Watai and Keiichi Katsumata for determining $CO_2$ and $CH_4$ concentrations of the reference gases used at HAT. We wish to thank Jiye Zeng for calculating backward trajectories. The $CO_2$ and $CH_4$ data for MLO sites are downloaded from www.esrl.noaa.gov/gmd – the contribution of GMD personnel is greatly appreciated. Two anonymous reviewers and O. R. Cooper made valuable comments, which were useful for improving the manuscript. This work was partly supported by the Grants-in-Aid for Creative Scientific Research (2005/17GS0203) of the Ministry of Education, Science, Sports and Culture, Japan.

Edited by: O. Cooper

## References

Akimoto, H., Ohara, T., Kurokawa, J., and Horii, N.: Verification of energy consumption in China during 1996–2003 by using satellite observational data, Atmos. Environ., 40, 7663–7667, 2006.

Andreae, M. O. and Merlet, P.: Emission of trace gases and aerosols from biomass burning, Global Biogeochem. Cy., 15, 955–966, 2001.

Conway, T. J., Tans, P. P., Waterman, L. S., Thoning, K. W., Kitzis, D. R., Masarie, K. A., and Zhang, N.: Evidence for interannual variability of the carbon cycle from the National Oceanic and Atmospheric Administration/Climate Monitoring and Diagnostics Laboratory Global Air Sampling Network, J. Geophys. Res., 99, 22831–22855, 1994.

Dlugokencky, E. J. D., Steele, L. P., Lang, P. M., and Masarie, K. A.: Atmospheric methane at Mauna Loa and Barrow observatories:

Presentation and analysis of in situ measurements, J. Geophys. Res., 100, 23103–23113, 1995.

Dlugokencky, E. J., Steele, L. P., Lang, P. M., and Masarie, K. A.: The growth rate and distribution of atmospheric methane, J. Geophys. Res., 99, 17021–17043, 1994.

Dlugokencky, E. J., Bruhwiler, L., White, J. W. C., Emmons, L. K., Novelli, P. C., Montzka, S. A., Masarie, K. A., Lang, P. M., Crotwell, A. M., and Miller, J. B.: Observational constraints on recent increase in the atmospheric $CH_4$ burden, Geophys. Res. Lett., 36, L18803, doi:10.1029/2009GL039780, 2009.

Eyring, V., Isaksen, I. S. A., Berntsen, T., Collins, W. J., Corbett, J. J., Endresen, O., Grainger, R. G., Moldanova, J., Schlager, H., and Stevenson, D. S.: Transport impacts on atmosphere and climate: Shipping, Atmos. Environ., doi:10.1016/j.atmosenv.2009.04.059, in press, 2010.

Gregg, J. S., Andres, R. J., and Marland, G.: China: Emissions pattern of the world leader in $CO_2$ emissions from fossil fuel consumption and cement production, Geophys. Res. Lett., 35, L08806, doi:10.1029/2007GL032887, 2008.

Houghton, R. A.: Revised estimates of the annual net flux of carbon to the atmosphere from changes in land use and land management 1850–2000, Tellus, 55B, 378–390, 2003.

Ito, A.: The regional carbon budget of East Asia simulated with a terrestrial ecosystem model and validated using AsiaFlux data, Agric. Forest. Meteorol., 148, 738–747, doi:10.1016/j.agrformet.2007.12.007, 2008.

Kanamitsu, M., Ebisuzaki, W., Woolen, J., Potter, J., and Fiorino, M.: NCEP/DOE AMIP-II Reanalysis (R-2), B. Am. Meteorol. Soc., 83, 1631–1643, 2002.

Kasischke, E. S., Hyer, E. J., Novelli, P. C., Bruhwiler, L. P., French, N. H. F., Sukhinin, A. I., Hewson, J. H., and Stocks, B. J.: Influences of boreal fire emissions on Northern Hemisphere atmospheric carbon and carbon monoxide, Global Biogeochem. Cy., 19, GB1012, doi:10.1029/2004GB002300, 2005.

Keeling, C. D., Whorf, T. P., Wahlen, M., and van der Plicht, J.: Interannual extremes in the rate of rise of atmospheric carbon dioxide since 1980, Nature, 375, 666–670, 1995.

Kistler, R., Kalnay, E., Collins, W., Saha, S., White, G., Woollen, J., Chelliah, M., Ebisuzaki W., Kanamitsu, M., Kousky, V., van den Dool, H., Jenne, R., and Fiorino, M.: The NCEP-NCAR 50-Year Reanalysis: Monthly means CD-ROM and documentation, Bull. Am. Meteorol. Soc., 82, 247–268, 2001.

Law, R. M., Peters, W., Rödenbeck, C., Aulagnier, C., Baker, I., Bergmann, D. J., Bousquet, P., Brandt, J., Bruhwiler, L., Cameron-Smith, P. J., Christensen, J. H., Delage, F., Denning, A. S., Fan, S., Geels, C., Houweling, S., Imasu, R., Karstens, U., Kawa, S. R., Kleist, J., Krol, M. C., Lin, S.-J., Lokupitiya, R., Maki, T., Maksyutov, S., Niwa, Y., Onishi, R., Parazoo, N., Patra, P. K., Pieterse, G., Rivier, L., Satoh, M., Serrar, S., Taguchi, S., Takigawa, M., Vautard, R., Vermeulen, A. T., and Zhu, Z.: TransCom model simulations of hourly atmospheric $CO_2$: Experimental overview and diurnal cycle results for 2002, Global Biogeochem. Cy., 22, GB3009, doi:10.1029/2007GB003050, 2008.

Machida, T., Katsumata, K., Tohjima, Y., Watai, T., and Mukai, H.: Preparing and maintaining of $CO_2$ calibration scale in National Institute for Environmental Studies-NIES 95 $CO_2$ scale, in Report of the 14th WMO Meeting of Experts on Carbon Dioxide Concentration and Related Tracer Measurement Techniques, Helsinki, Finland, 10–13 September 2007, WMO/GAW Rep. 186, edited by: Laurila, T., 26–29, WMO, Geneva, Swizerland, 2009.

Marland, G., Boden, T. A., and Andres, R. J.: Global, regional, and national $CO_2$ emissions, Carbon Dioxide Inf. Anal. Cent., Oak Ridge Natl. Lab., US Dep. Of Energy, Oak Ridge, Tenn. (http://cdiac.ornl.gov/trends/emis/tre/regn.html), 2007.

Mukai, H., Katsumoto, M., Ide, R., Machida, T., Fujinuma, Y., Nojiri, Y., Inagaki, M., Oda, N., and Watai, T.: Characterization of atmospheric $CO_2$ observed at two-background air monitoring stations (Hateruma and Ochi-ishi) in Japan (abstract), paper presented at Sixth International Carbon Dioxide Conference, Organ. Comm. of Sixth Int. Carbon Dioxide Conf., Sendai, Japan, 2001.

Newell, R. E. and Evans, M. J.: Seasonal changes in pollutant transport to the North Pacific: the relative importance of Asian and European sources, Geophys. Res. Lett., 27, 2509–2512, 2000.

Ohara, T., Akimoto, H., Kurokawa, J., Horii, N., Yamaji, K., Yan, X., and Hayasaka, T.: An Asian emission inventory of anthropogenic emission sources for the period 1980–2020, Atmos. Chem. Phys., 7, 4419–4444, 2007, http://www.atmos-chem-phys.net/7/4419/2007/.

Olivier, J. G. J. and Berdowski, J. J. M.: Global emissions sources and sinks, in: The Climate system, edited by: Berdowski, J., Guicherit, R., and Heij, B. J., A. A. Balkema Publishers/Swets & Zeitlinger Publishers, Lisse, The Netherlands, ISBN 9058092550, 33–78, 2001.

Olivier, J. G. J., Van Aardenne, J. A., Dentener, F., Ganzeveld, L., and Peters, J. A. H. W.: Recent trends in global greenhouse gas emissions: regional trends and spatial distribution of key sources, in: "Non-$CO_2$ Greenhouse Gasses (NCGG-4)", A. van Amstel (coord.), 325–330, Millpress, Rotterdam, ISBN 9059660439, 2005.

Patra, P. K., Maksyutov, S., and Nakazawa, T.: Analysis of atmospheric $CO_2$ growth rates at Mauna Loa using $CO_2$ fluxes from an inverse model, Tellus, 57B, 357–365, 2005.

Patra, P. K., Low, R. M., Peters, W., Rödenbeck, C., Takigawa, M., Aulagnier, C., Baker, I., Bergmann, D. J., Bousquet, P., Brandt, J., Bruhwiler, L., Cameron-Smith, P. J., Christensen, J. H., Delage, F., Denning, A. S., Fan, S., Geels, C., Houweling, S., Imasu, R., Karstens, U., Kawa, S. R., Kleist, J., Krol, M. C., Lin, S.-J., Lokupitiya, R., Maki, T., Maksyutov, S., Niwa, Y., Onishi, R., Parazoo, N., Pieterse, G., Rivier, L., Satoh, M., Serrar, S., Taguchi, S., Vautard, R., Vermeulen, A. T., and Zhu, Z.: TransCom model simulations of hourly atmospheric $CO_2$: Analysis of synoptic-scale variations for the period 2002–2003, Global Biogeochem. Cy., 22, GB4013, doi:10.1029/2007GB003081, 2008.

Patra, P. K., Takigawa, M., Ishijima, K., Choi, B.-C., Cunnold, D., Dlugokencky, E. J., Fraser, P., Gomez-Pelaez, A. J., Goo, T.-Y., Kim, J.-S., Krummel, P., Langenfelds, R., Meinhardt, F., Mukai, H., O'Doherty, S., Prinn, R. G., Simmonds, P., Steele, P., Tohjima, Y., Tsuboi, K., Uhse, K., Weiss, R., Worthy, D., and Nakazawa, T.: Growth rate, seasonal, synoptic, diurnal variations and budget in lower atmospheric methane, J. Meteorol. Soc. Japan, 87, 635–663, doi:10.2151/jmsj.87.635, 2009.

Randerson, J. T., Thompson, M. V., Conway, T. J., Fung, I. Y., and Field, C. B.: The contribution of terrestrial sources and sinks to trends in the seasonal cycle of atmospheric carbon dioxide, Global Biogeochem. Cy., 11(4), 535–560, 1997.

Raupach, M., Marland, G., Ciais, P., Le Quere, C., Canadell, J. G., Klepper, G., and Field, C.: Global and regional drivers of accelerating $CO_2$ emissions, Proc. Natl. Acad. Sci. USA, 104, 10288–10293, 2007.

Simpson, I. J., Rowland, F. S., Meinardi, S., and Blake, D. R.: Influence of biomass burning during recent fluctuations in the slow growth of global tropospheric methane, Geophys. Res. Lett., 33, L22808, doi:10.1029/2006GL027330, 2006.

Takahashi, T., Sutherland, S. C., Wanninkhof, R., Sweeney, C., Feely, R. A., Chipman, D. W., Hales, B., Friederich, G., Chavez, F., Sabine, C., Watson, A., Bakker, D. C. E., Schuster, U., Metzl, N., Yoshikawa-Inoue, H., Ishii, M., Midorikawa, T., Nojiri, Y., Körtzinger, A., Steinhoff, T., Hoppema, M., Olafsson, J., Arnarson, T. S., Tilbrook, B., Johannessen, T., Olsen, A., Bellerby, R., Wong, C. S., Delille, B., Bates, N. R., and de Baar, H. J. W.: Climatological mean and decadal change in surface ocean $pCO_2$, and net sea-air $CO_2$ flux over the global oceans, Deep-Sea Res. Pt. II, 56, 554–577, doi:10.1016/j.dsr2.2008.12.009, 2009.

Tans, P. P., Fung, I. Y., and Takahashi, T.: Observational constraints on the global atmospheric $CO_2$ budget, Science, 247, 1431–1438, 1990.

Thoning, K. W., Tans, P. P., and Komhyr, W. D.: Atmospheric carbon dioxide at Mauna Loa Observatory 2. Analysis of the NOAA GMCC data, 1974–1985, J. Geophys. Res., 94, 8549–8565, 1989.

Tohjima, Y., Mukai, H., Maksyutov, S., Tkahashi, Y., Machida, T., Katsumoto, M., and Fujinuma, Y.: Variations in atmospheric nitrous oxide observed at Hateruma monitoring station, Chemosphere, 2, 435–443, 2000.

Tohjima, Y., Machida, T., Utiyama, M., Katsumoto, M., and Fujinuma, Y.: Analysis and presentation of in situ atmospheric methane measurements from Cape Ochi-ishi and Hateruma Island, J. Geophys. Res., 107, D12, doi:10.1029/2001JD001003, 2002.

Trenberth, K. E.: The definition of El Niño, Bull. Am. Meteorol. Soc., 78, 2771–2777, 1997.

Yan, X., Cai, Z., Ohara, T., and Akimoto, H.: Methane emission from rice fields in mainland China: Amount and seasonal and spatial distribution, J. Geophys. Res., 108(D16), 4505, doi:10.1029/2002JD003182, 2003.

Yokouchi, Y., Taguchi, S., Saito, T., Tohjima, Y., Tanimoto, H., and Mukai, H.: High frequency measurements of HFCs at a remote site in east Asia and their implications for Chinese emissions, Geophys. Res. Lett., 33, L21814, doi:10.1029/2006GL026403, 2006.

Zeng, J., Tohjima, Y., Fujinuma, Y., Mukai, H., and Katsumoto, M.: A study of trajectory quality using methane measurements from Hateruma Island, Atmos. Environ., 37, 1911–1919, 2003.

Zhang, Q., Streets, D. G., He, K., Wang, Y., Richter, A., Burrows, J. P., Uno, I., Jang, C. J., Chen, D., Yao, Z., and Lei, Y.: $NO_x$ emission trends for China, 1995–2004: The view from the ground and the view from space, J. Geophys. Res., 112, D22306, doi:10.1029/2007JD008684, 2007.

Zhou, L. X., Kitzis, D., and Tans, P. P.: Report of the fourth WMO Round-Robin reference gas intercomparison, 2002–2007, in Report of the 14th WMO Meeting of Experts on Carbon Dioxide Concentration and Related Tracer Measurement Techniques, Helsinki, Finland, 10–13 September 2007, WMO/GAW Rep. 186, edited by: Laurila, T., 40–43, WMO, Geneva, Swizerland, 2009.